ENVIRONMENTAL DEPENDENCE OF WARPS IN SPIRAL GALAXIES

HONG BAE ANN AND HYUN JEONG BAE

Pusan National University, Busandaehak-ro 63beon-gil, Geumjeong-gu, Busan 46241, Korea; hbann@pusan.ac.kr

Abstract: We determined the warp parameters of 192 warped galaxies which are selected from 340 edge-on galaxies using color images as well as r-band isophotal maps. We derive the local background density (Σ_n) to examine the dependence of the warp amplitudes on the galaxy environment. We find a clear trend that strongly warped galaxies are likely to be found in high density regions where tidal interactions are supposed to be frequent. However, the correlation between α_w and Σ_n is too weak for weakly warped galaxies ($\alpha_w < 4°$) and the cumulative distributions of weakly warped galaxies are not significantly different from those of galaxies with no detectable warps. This suggests that tidal interactions do not play a decisive role in the formation of weak warps.

Key words: galaxies: general – galaxies: morphology – galaxies: spiral – galaxies: structure

1. INTRODUCTION

Many spiral galaxies have warped disks. Warped disks are observed by radio band (HI warp) and optical band (stellar warp). HI warps extend beyond the stellar disks (Sancisi 1976; Garcia-Ruiz et al. 2002), sometimes up to 100 kpc, displaying conspicuous features (Bosma 1981a,b; Reshetnikov et al. 2002). Stellar warps are much less conspicuous than HI warps and are difficult to detect in most cases. Warps are also observed in the 4.5 μ band (Saha et al. 2009). By optical observations, approximately 50% of all disk galaxies have stellar warps (Sanchez-Saavedra et al. 1990; Reshetnikov & Combes 1998; Ann & Park 2006). The structural properties of warped disks can be quantified by the warp angle (α_w), warp radius (r_w), and warp asymmetry. In general, a warp angle is defined as the angle between the major axis and the line connecting the center of the galaxy and the terminal point of the warp, while the warp radius is defined as the radius at which the disk begins to bend. Warp asymmetry denotes the degree of asymmetry between warps in opposite directions. It is more frequent in small scale length systems (van der Kruit & Freeman 2011). The study by Ann & Park (2006) showed that the warp angle is inversely proportional to the warp radius, but is proportional to warp asymmetry.

There have been many studies about the origin and maintenance mechanisms of warps. The mechanisms driving warps are divided into two categories: internal and external mechanisms. Internal mechanisms are due to gravitational torques from internal structures, such as misaligned halos (Kuijken 1991; Debattista & Sellwood 1999; Ideta et al. 2000; Bailin & Steinmetz 2005a; Dubinski & Chakrabatry 2009; Jeon et al. 2009), or bending modes (Lyndenn-Bell 1965; Spark & Casertano 1988; Revaz & Pfenniger 2004). External mechanisms include tidal forces by satellites or fly-by galaxies

CORRESPONDING AUTHOR: H. B. Ann

(Quinn, Hernquist, & Fullagar 1993; Huang & Carlberg 1997; Bailin & Steinmetz 2005b; Kalirai et al. 2006; Weinberg & Blitz 2006; Kim et al. 2014; Gomez 2016) or the accretion of intergalactic materials (Ostriker & Binney 1989; Jiang & Binney 1999; Lopez-Corredoira et al. 2002; Sanchez-Salcedo 2006; Shen & Sellwood 2006), especially by misaligned infall from the cosmic web or a cooling gas halo (Roskar et al. 2010; Aumer et al. 2013). Intergalactic magnetic fields (Battaner et al. 1990, 1998) are also thought to drive warps, especially the HI warps. Since all the proposed mechanisms require some assumptions about the conditions for disk warping, statistical studies of the warped disks could play a usfull role in constraining assumptions about the formation of warps.

There are several statistical studies of warped disks, including the fraction of warped disks (Sanchez-Saavedra et al. 1990; Reshetnikov & Combes 1998; Castro-Rodriguez et al. 2002; Ann & Park 2006). These studies showed that more than half of all disk galaxies have warped disks, and that S-shaped warps are most popular. The warp frequency is thought to depend on the environment in the sense that warped galaxies are more frequent in rich environment than in poor environment (Reshetnikov & Combes 1998, 1999). The higher frequency of warps in rich environment indicates that warps are caused by tidal interactions. The high fraction of warped disks in merging systems (Schwarzkopf & Dettmar 2001) supports the tidal origin of the warps. However, Garcia-Ruiz et al. (2002) reported a higher frequency of warps in poor environment than in rich environment. Thus, clarifying the relation between warp frequency and galaxy environment is important to understand the origin of warps.

The present study is focused on the environment of warped disks. The environment of a galaxy is as important as the mass of a galaxy since the formation and evolution of a galaxy depend on both the environment and the mass. The environment measure we consider
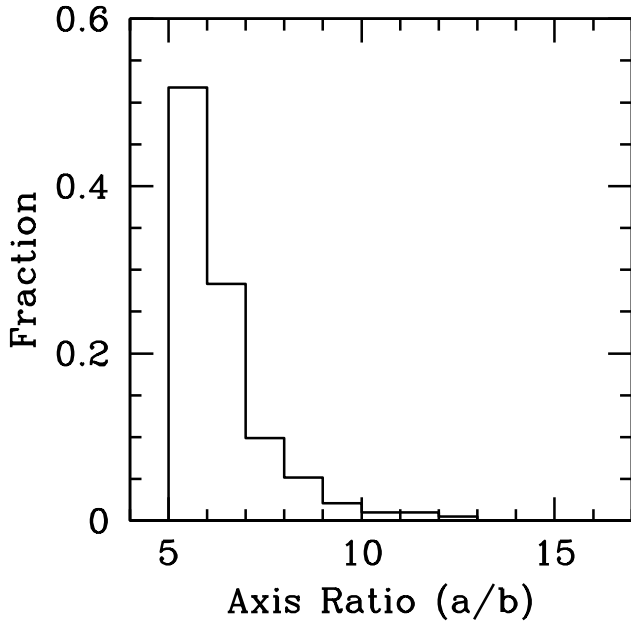
Figure 1. Axis ratio distributions of the 192 warped galaxies. The major axis length (a) and minor axis length (b) are derived from the r-band isophotal maps.

Figure 2. Color images of sample galaxies. Warps with prototypical shapes are displayed in the first three rows; the first row shows L-shaped warps, the second row shows U-shaped warps, and the third row shows S-shaped warps. Peculiar warps are shown in the fourth row. The number in the upper right corner of each panel is the warp angle (α_w) defined in the text.

is the local background density Σ_n derived from the projected distances to the nth nearest neighbor galaxies. It is closely related to disk morphology. For example, early type spiral galaxies are likely to be found in high density regions while late type spiral galaxies are frequently found in low density regions. Arm classes are also related to the local background in the sense that two-armed grand designs are preferentially found in high density regions, while flocculent arms are mostly in low density regions (Ann 2013, 2014). Since stellar warps are the deformation of a stellar disk driven by internal/external gravitational forces, we expect that the local background density is closely related to warp phenomena. Thanks to redshift data in the Sloan Digital Sky Survey (SDSS), it is now possible to derive the local background density of a galaxy using a volume-limited sample.

The purpose of the present study is to clarify whether environmental effects are important for the formation of warps. To do this, we construct a sample of 192 warped galaxies. We consider galaxies with warp angles greater than a certain value, which is set by consideration of measurement errors. We used weakly warped galaxies ($\alpha_w < 4°$) as a comparison sample in a statistical analysis of the environmental dependence of warp amplitude.

This paper is organized as follows. Section 2 describes the sample and measurement of warp parameters. Section 3 presents the properties of warped disks. Section 4 describes the relationship between the environment and warp amplitude, and the conclusions with discussion are given in Section 5.
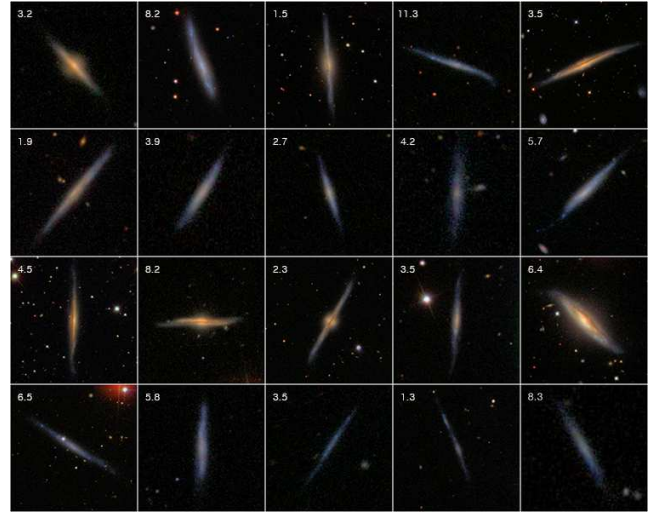
2. OBSERVATIONAL DATA

2.1. Sample Selection

The sample galaxies of the present study came from the Korea Institute of Advanced Study (KIAS) Value-Added Galaxy Catalog (VAGC) of Choi et al. (2010), which was derived from the New York University VAGC DR7 (NYU VAGC; Blanton et al. 2005). The basic data in these catalogs are derived from the SDSS DR7 (Abazajian et al. 2009). The KIAS VAGC supplements bright galaxies, which have no SDSS spectroscopic redshift, using various redshift catalogs including the NASA Extragalactic Database (NED). Thus, the KIAS VAGC provides redshifts of a nearly complete sample of galaxies brighter than $r_{petrosian} = 17.77$. We first extracted 26,246 galaxies with redshifts less than $z = 0.025$ from the KIAS VAGC. Some entries in the KIAS VAGC are not of a real galaxy, but part of a galaxy. Some are duplicated entries with slightly offset coordinates. We removed these entries from the galaxies in the KIAS VAGC to make a clean sample of 25,999 galaxies with spectroscopic redshifts less than $z = 0.025$. From this sample, we select 2,298 galaxies as candidate edge-on galaxies by visual inspection of the color images from the SDSS DR7.

The final sample of 340 edge-on galaxies was selected by the axis ratio (a/b) measured from the r-band isophotal maps, which were derived by conducting a surface photometry of the galaxies using the calibrated images. We followed the general procedures of galaxy surface photometry. We used the mode of observed intensity around the target galaxy for the subtraction of the local sky background. Gaussian smoothing is then applied to reduce the noise in the isophotal maps. We then calibrated the present photome-
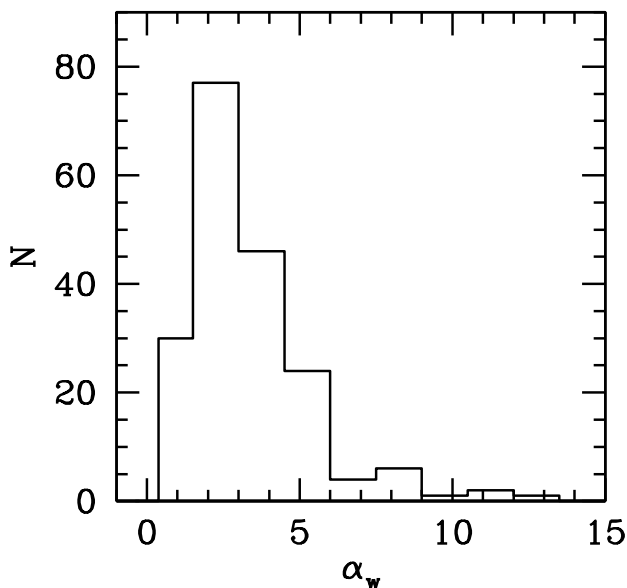
Figure 3. Number distribution of warp angles (α_w).

Figure 4. Luminosity distribution of 340 edge-on galaxies. warped galaxies are plotted by solid line while the luminosity function of galaxies with no detectable warps are indicated by dotted line.

try using the intensity of the background sky represented by maggie/arcsec^2, which was downloaded from the SDSS DR7. In most cases, the surface brightness of the outermost isophote is $\mu(r) = 26.5$ mag/arcsec^2, although in some galaxies, it is as bright as $\mu(r) = 24.5$ mag/arcsec^2 due to bright neighbor objects. Thus, disk axis lengths and warp parameters are measured at $\mu(r) \sim 26.5$ mag/arcsec^2. The final sample of 340 edge-on galaxies have axis ratios a/b greater than 5. In measuring the semi-minor axis lengths, we corrected for the effect of the central bulges if they are big enough to affect the light distribution along the disk minor axis by extrapolating the outermost isophotes beyond the bulge regions toward the center. We did not take into account other properties of galaxies, such as size and luminosity.

From the 340 edge-on galaxies, we first identified 160 warped disks through visual inspection of the isophotal maps. To this warped galaxy sample, we add 32 galaxies which are found to have warped disks by inspecting the color images of the galaxies using the SDSS Navigate Tool. Most of the 32 galaxies additionally found from the color images are weak L-shaped warps. The reason these galaxies were missed in the visual inspection of the isophotal maps is the low resolution of the isophotal maps, which prevents the detection of fine structures. From the isophotal maps, we could identify warps with $\alpha_w \gtrsim 1.5°$. The zoom-in and zoom-out function of the SDSS Navigate Tool also helps to identify weak warps. We decided to identify warped galaxies by imposing a constraint for the minimum angle to detect warps ($\alpha_{w,min}$). This is possible because we could measure warp angles as small as $\sim 0.2°$ using the coordinates of the cursor position. We use the SDSS DR7 Navigate Tool to measure the coordinates of the center of the galaxy, the point at which the disk begins to bend (warp radius), and the tip of
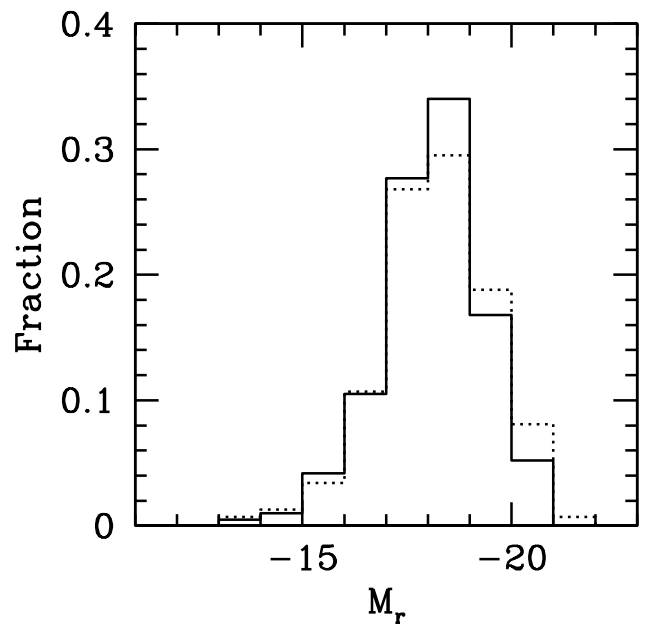
the warped disk in either side of the disk. The number of warped galaxies identified from the color image is 192 with $\alpha_{w,min}$ as 1°. The number of warped galaxies depends on $\alpha_{w,min}$. It is 218 for $\alpha_{w,min} = 0.5°$ and 161 for $\alpha_{w,min} = 1.5°$. The number of warped galaxies identified with $\alpha_{w,min} = 1.5°$ is similar to that identified from the isophotal maps. In any case, the majority of warps are identified as L-shaped warps. We adopt the 192 warped galaxies from the color images as the final sample of warped galaxies. Figure 1 shows the axis ratio distributions of the 192 warped disks. It shows the highest peaks at the first bin, which is the bin of the smallest axis ratio. The majority of warped disks have axis ratios less than $a/b = 7$.

There are three warp types: S-shaped, U-shaped, and L-shaped. The S-shaped warps show the outer part of the edge-on disks bent in opposite directions, displaying a point-symmetric shape; U-shaped warps bend in the same direction, displaying an axis-symmetric shape. The L-shaped warps show appreciable warp only in one side of their disks; L-shaped warps were the most frequent warp type found in the present sample. In Figure 2, we present some prototypical examples of warp morphology together with warps in extremely thin disks. As can be seen in Figure 2, most warps are not very prominent. Among the three types of warps, the S-shaped warps are likely to have a pronounced warp, while the U-shaped warps are not. The fraction of U-shaped warps is much smaller than the fraction of L-shaped and S-shaped warps. Most of the warp driving mechanisms apply to S-shaped warps while only a few mechanisms are relevant to the U-shaped warps. One of the promising models that explain the U-shaped warps
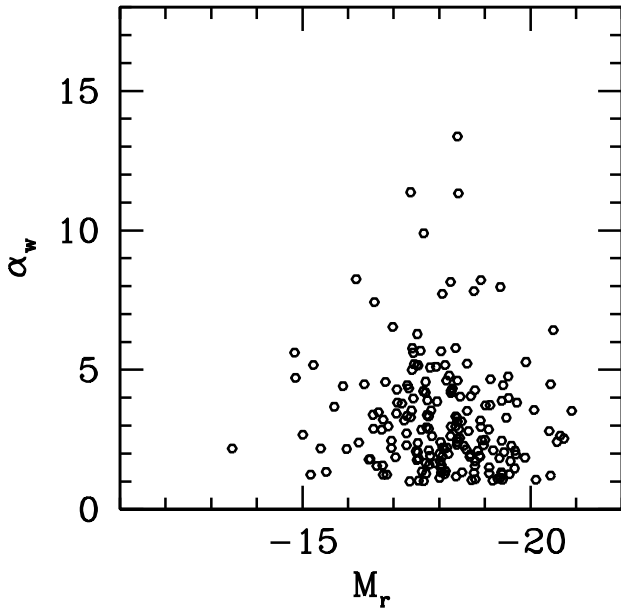
Figure 5. Relation between the warp angle (α_w) and galaxy luminosity (M_r).

is that of Sanchez-Salcedo (2006) which predicts that U-shaped warps are generally weak and less frequent than S-shaped warps. Also, U-shaped warps are very rare in early type spiral galaxies. It is worth noting that a non-negligible fraction of warped galaxies shows a wavy pattern along the major axis of the disk. Similar wavy patterns in warped disks was reported in the HI observations too (Garcia-Ruiz et al. 2002). This wavy pattern leads to misclassification of warp type between U-shaped warp and S-shaped warp. It also affects the measurement of warp angle. Some examples of warped disks that display the wavy pattern are given in the fourth column of Figure 2. Warps with a wavy pattern may be formed by the bending mode, as suggested by Lyndenn-Bell (1965).

2.2. Measurement of Warp Parameters

We determined the warp parameters and disk axis lengths using r-band isophotal maps, as well as color images using the SDSS DR7 Navigate Tool. The warp parameters we measured are the warp angle (α_w) and warp radius (r_w). α_w is used to represent the warp amplitude of a galaxy because it is assumed to be closely related to the warp-driving force. There is a clear tendency that r_w of strongly warped galaxies, which have a large α_w, is smaller than r_w of weakly warped galaxies (Ann & Park 2006). However, r_w is not well defined in some cases due to the wavy patterns and the inherent asymmetry in the disk major axis length. This is the reason why we use α_w rather than r_w in the investigation of the environmental dependence of warp parameters, which is discussed in section 4. We measured r_w directly from the images, but we derived α_w from the height and base of the right-angled triangle connecting the center of the galaxy, the tip of the warped disk, and the point where a vertical line from the tip meets the
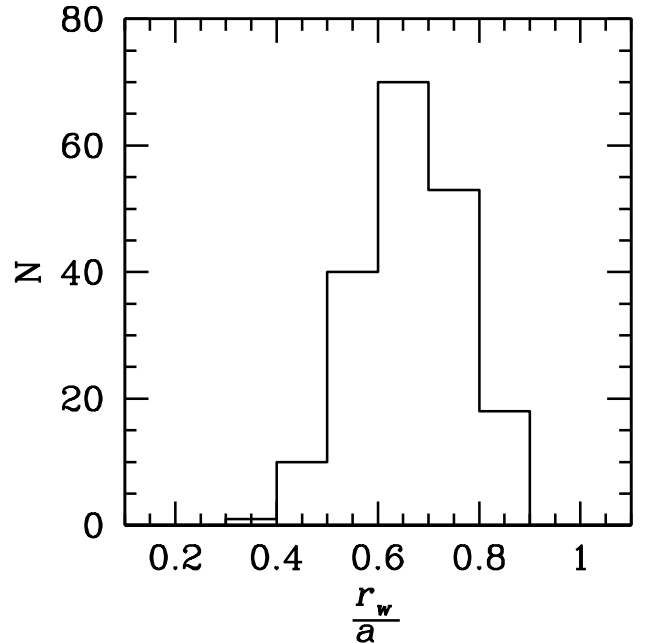

Figure 6. Frequency distribution of the ratio between the warp radius and the semi-major axis length (r_w/a).

major axis of the disk. We suppose that the length of the base is roughly the same as the semi-major axis (a) of the disk.

To determine the warp parameters from the isophotal maps, the center of a galaxy is assigned to the center of the brightest isophotes unless it deviates from the center of the symmetrical luminosity distribution. In cases in which the brightest isophotes do not suggest the center of the galaxy, we take the center of the second brightest isophotes as the center of the galaxy. In colour images, we select the center of a galaxy as the center of the symmetric light distribution of the inner part of the disk using the image display tools. It usually coincides with the brightest point of the galaxy. In any case, defining the mean major axis of a disk is as important as selecting the center of the galaxy in the measurement of the warp parameters because the largest source of errors associated with the parameter measurements comes from the errors in determining the major axis. The practical method that we adopted is to draw a line connecting the center of the galaxy and the warp radius before measuring the relevant lengths. This method is used to measure the parameters from the isophotal maps. When measuring the parameters using the SDSS Navigate Tool, the mean major axis was defined by extrapolating the line connecting the center of the galaxy and the warp radius using their coordinates. Thus, the position of the warp radius is selected to allow for the most plausible disk mean major axis when connected to the galaxy center. The errors caused by the uncertainties in the mean major axis are as large as $\sim 3°$ when the major axis of the disk is heavily curved.

The procedure used to measure α_w from the color images using the SDSS Navigate Tool is slightly differ-

Table 1
Morphology and warp type distributions of 340 edge-on galaxies

Type	L	U	S	no warp
S0	0	0	0	2
e	6	1	3	1
i	27	2	11	38
l	79	14	49	107

ent from that using isophotal maps. While the height and base of the right-angled triangle could be measured by a ruler or by a cursor, they could be calculated from measuring the coordinates of the three points (galaxy center, warp radius, and tip of the warp) using simple analytic geometry. We found that the warp angles measured from the isophotal maps had errors that were slightly larger than the errors created using the Navigate Tool. This is due to the large errors associated with measuring lengths using a ruler. Thus, we adopt the warp radii and warp angles of the 340 edge-on galaxies measured by the SDSS Navigate Tool as the fiducial data for the warp parameters.

3. BASIC PROPERTIES OF WARPED DISKS

3.1. Warp Types

The 192 warped galaxies are characterized as one of the three warp types: S-shaped, U-shaped, or L-shaped. The three symbols for the warp types resemble the shape of the warps. In other words, the S-shaped warp has a symmetric shape that bends in opposite directions, while the U-shaped warp bends in the same direction. The L-shaped warp displays a warp only in one side of the disk. The L-shaped warp was first noticed by Sanchez-Saavedra et al. (2003). There are 63 S-shaped warps, 17 U-shaped warps, and 112 L-shaped warps. However, the number of warps detected depends on the minimum warp angle $\alpha_{w,min}$ to be identified as a warp. We used $\alpha_{w,min} = 1.0°$ which is the mean measurement error of warp angles. We examined two other choices of $\alpha_{w,min}$ (0.5° and 1.5°) to see the effect on the detection of warps. The number of warped galaxies for $\alpha_{w,min} = 0.5$ and $\alpha_{w,min} = 1.5$ are 218 and 161, respectively. That is, they yield $\sim 15\%$ increase or decrease in the number of warped galaxies. The fraction of warped galaxies (56%) is similar to that of Sanchez-Saavedra et al. (2003) but somewhat smaller than those of Reshetnikov & Combes (1998) and Ann & Park (2006) who reported $\sim 70\%$ of edge-on spiral galaxies have warps. The reason for the discrepancy between ours and those of Reshetnikov & Combes (1998) and Ann & Park (2006) is the selection criterion for the axis ratio. We used $a/b > 5$ while $a/b = 7$ and $a/b = 9.5$ were used by Reshetnikov & Combes (1998) and Ann & Park (2006), respectively. If we consider the galaxies with $a/b > 7$, then the warp fraction of the present sample is $\sim 65\%$. The dominance of L-shaped warps in the present study is partly due to the small cut-off value of $a/b = 5$. We suppose that the majority

of the L-shaped warps would be classified as S-shaped warps with high asymmetry. Actually, most of the additional warps detected by imposing $\alpha_{w,min} = 0.5°$ are S-shaped warps.

3.2. Warp Angle

There are two kinds of warp angle, α_w and β_w, (Ann & Park 2006). The former (α_w) has been widely used to represent the warp amplitude (Sanchez-Saavedra et al. 1990; Reshetnikov & Combes 1998; Garcia-Ruiz et al. 2002; Sanchez-Saavedra et al. 2003; Ann & Park 2006). The latter (β_w) was used by Sanchez-Saavedra et al. (2003) and Ann & Park (2006) but was not considered as a proxy of the warp amplitude because of its dependence on the warp radius, which is most uncertain owing to the frequent wavy pattern along the major axis (Ann & Park 2006). Thus, we assumed the α_w as a proxy of the warp amplitude and used the larger α_w between the two if the two warp angles α_w in the opposite side of a disk are different.

The mean warp angle of 192 warped galaxies is $3.3° \pm 1.0°$ which is much smaller than those of earlier studies (Sanchez-Saavedra et al. 1990, 2003) but very similar to that of Ann & Park (2006). The frequency distribution of α_w is plotted in Figure 3. The majority ($\sim 70\%$) of the warped galaxies have α_w between 2° and 6°. The strongly warped galaxies ($\alpha_w > 4°$) comprise $\sim 30\%$ of warped galaxies. They are considered to be strong warps in the sense that they are easy to identify by visual inspection. This limiting warp angle for strong warps is about four times larger than the mean error of the warp angle.

Figure 4 shows that the luminosity distribution of warped galaxies is not significantly different from that of galaxies with no detectable warp. M_r is the absolute $r-$band magnitude corrected for the galactic extinction. We used the Hubble constant of $H=75$ km s^{-1} to derive the distances of galaxies using the redshift corrected for the motion relative to the centroid of the LG following the prescription of Mould et al. (2000). For the galaxies in the direction of the Virgo cluster with redshift less than $z = 0.007$, the distance of the Virgo cluster (16.7 Mpc) was used following Kraan-Korteweg (1986). As shown in Figure 5, there seems to be no dependence of the warp angle (α_w) on the galaxy luminosity. The irrelevance of the galaxy luminosity and warp amplitude implies that the warp driving mechanisms are not much dependent on the internal properties of a galaxy. However, the warp phenomena are not free from the effects of the internal properties of a galaxy when the disk and halo of a galaxy are misaligned. Debattista & Sellwood (1999) were the first who showed that misaligned halo easily drive S-shaped warps using N-body simulations. Ideta et al. (2000) and Jeon et al. (2009) confirmed S-shaped warps driven by the misaligned halo in a variety of conditions.

3.3. Warp Radius

There have been no detailed statistics on the warp radius except for the analysis of warp radius by Ann &

Table 2
Warp parameters and environment measures of 192 warped galaxies

ID	α_{2000}	δ_{2000}	D (Mpc)	M_r	a/b	T[a]	Warp	α_w (°)	r_w (kpc)	r_w/a	Σ_7' [b]	SDSS name
65626	211.1057	-0.4568	95.7	-18.78	5.49	i	S	4.3±0.4	5.7	0.6	0.53	J140425.37-002724.3
149665	9.9097	14.6642	71.7	-18.90	5.21	e	U	3.2±0.2	3.3	0.8	-0.17	J003938.31+143951.2
175799	189.7713	-2.4836	89.3	-17.40	5.24	l	L	5.0±0.5	1.5	0.5	0.14	J123905.11-022900.7
192401	118.4393	39.7827	49.7	-17.30	6.29	l	S	4.5±1.7	9.4	0.7	0.41	J075345.26+394657.4
209810	134.7826	53.6324	27.6	-17.59	5.72	l	L	5.7±0.5	7.5	0.6	0.49	J085907.81+533756.5
225194	115.1637	39.2333	42.8	-20.58	5.15	i	L	2.4±0.5	35.1	0.8	-0.45	J074039.28+391359.8
234754	166.6193	67.4902	80.1	-18.67	5.18	l	U	1.9±0.8	11.3	0.6	-0.73	J110628.61+672924.4
254494	236.3260	57.4097	52.1	-18.16	5.32	l	L	4.6±0.6	6.6	0.5	-0.55	J154518.23+572434.9
263459	192.6623	1.4645	14.7	-17.35	5.48	l	L	1.0±1.0	24.5	0.8	1.08	J125038.95+012752.2
269490	228.0090	1.6977	25.9	-16.98	7.56	l	L	6.5±2.7	13.1	0.6	1.01	J151202.18+014151.4
289096	187.8359	3.1249	67.2	-17.84	5.32	l	L	2.6±0.5	0.4	0.6	-0.19	J123120.62+030729.6
289369	198.7750	3.0452	85.2	-19.70	5.24	i	U	3.8±0.5	5.0	0.7	-0.23	J123120.62+030729.6
305252	236.6008	2.8442	20.2	-15.70	5.23	l	S	3.7±1.3	4.9	0.6	-0.15	J154624.23+025039.1
325017	30.7585	-9.6563	53.3	-18.71	8.47	l	L	1.0±1.5	19.2	0.7	-0.07	J020302.05-093922.6
380333	24.6619	13.7179	92.2	-17.49	6.83	l	L	2.1±0.5	2.7	0.7	-0.23	J013838.86+134304.2
383654	3.4114	15.6751	28.6	-15.52	8.53	l	L	1.3±1.3	7.1	0.3	-1.31	J001338.62+154029.5
472152	125.3485	41.7075	95.9	-17.33	8.11	e	L	4.3±0.4	2.2	0.8	-0.37	J082123.62+414226.8
525670	206.0022	4.7345	90.7	-17.41	5.31	l	S	5.8±2.1	2.6	0.7	0.70	J134400.54+044404.2
528224	186.7875	5.8801	16.7	-18.25	5.47	l	S	8.2±1.9	9.9	0.6	1.33	J122708.99+055248.2
532646	246.2369	46.5988	95.0	-18.01	5.49	l	S	2.0±1.0	2.6	0.6	-0.56	J162456.83+463555.7
545583	180.5854	63.1209	80.9	-18.36	5.22	l	L	3.0±1.8	16.6	0.8	-0.55	J120220.47+630715.2
599912	236.6068	4.4274	43.2	-17.54	6.23	l	L	5.2±2.0	6.7	0.7	-0.81	J154625.63+042538.7
729862	261.4096	59.4468	72.8	-18.49	5.40	l	S	3.1±0.4	9.9	0.6	-0.74	J172538.29+592648.5
849575	118.9183	28.7430	83.4	-17.39	6.35	l	S	3.5±0.5	7.9	0.7	0.08	J075540.38+284435.1
862661	134.7440	39.2117	5.7	-13.46	7.04	l	L	2.2±0.7	12.5	0.7	-0.23	J085858.54+391241.9
874733	148.1760	42.8787	59.7	-17.37	5.65	l	S	11.4±2.8	4.8	0.6	0.54	J095242.24+425242.6
925800	157.3146	6.1280	44.9	-18.88	6.09	i	L	1.9±0.2	16.3	0.7	-0.36	J102915.49+060741.0
927963	153.9028	6.3478	55.0	-17.28	5.33	l	L	2.7±0.6	5.0	0.6	-0.63	J101536.68+062052.1
937996	172.1294	9.1044	81.7	-20.08	6.46	i	S	3.6±0.6	2.6	0.7	0.73	J112831.04+090615.8
938047	173.4486	9.0710	79.7	-17.04	5.08	l	L	1.9±0.8	4.1	0.7	0.12	J113347.66+090415.5
947500	189.6557	10.4759	95.2	-20.41	12.71	i	L	2.8±0.2	10.4	0.7	-0.20	J123837.33+102833.1
950120	186.8428	10.8668	16.7	-17.66	5.95	l	L	1.0±0.9	9.9	0.7	1.70	J122722.25+105200.4
985396	235.6008	41.6235	91.6	-19.01	5.33	l	L	3.7±1.1	5.8	0.5	0.15	J101536.68+062052.1
998997	251.7272	31.8856	63.1	-17.77	7.70	l	S	2.1±0.3	8.3	0.8	-1.21	J112831.04+090615.8
1000378	228.8838	49.6207	32.6	-15.89	5.30	l	S	4.4±0.6	5.6	0.6	-0.12	J113347.66+090415.5
1061318	163.1393	10.0191	82.1	-19.51	5.14	i	L	4.8±1.1	5.5	0.4	0.32	J105233.41+100108.7
1126179	145.3837	11.4124	80.5	-19.58	5.57	i	S	2.3±0.6	29.1	0.8	0.86	J094132.08+112444.8
1155166	135.2302	31.9931	24.3	-16.49	5.73	l	L	1.8±1.2	14.1	0.8	0.36	J090055.24+315935.3
1163298	219.3066	43.6959	43.0	-18.97	7.41	l	S	2.3±0.5	15.6	0.8	-0.61	J143713.57+434145.3
1164346	225.9155	42.1263	67.9	-18.59	6.53	l	S	2.1±0.2	3.4	0.7	0.87	J150339.71+420734.6
1170711	174.3907	47.2092	96.5	-18.04	5.05	l	S	5.7±2.0	4.0	0.6	-0.40	J113733.74+471233.0
1244697	187.2760	44.6553	90.0	-20.65	6.28	i	S	2.6±1.4	9.7	0.6	0.49	J122906.24+443918.8
1283727	176.2508	7.4980	76.2	-18.36	5.68	l	S	5.8±2.3	4.0	0.5	0.38	J114500.21+072952.3
1285153	171.5585	7.8421	81.1	-19.37	6.94	l	S	2.5±0.1	6.4	0.6	-0.07	J112614.04+075031.4
1326762	192.7004	40.3036	62.2	-17.08	5.36	l	L	3.8±0.5	1.6	0.6	0.20	J125048.09+401812.8
1341995	183.9413	10.7024	16.7	-16.36	6.75	l	L	4.5±0.8	10.1	0.6	1.05	J121545.92+104207.6
1353316	210.6759	9.1641	76.3	-18.42	5.80	l	L	11.3±1.1	2.8	0.6	1.72	J140242.20+090950.9
1372341	230.3951	41.9052	71.3	-17.72	5.49	l	L	2.9±0.4	5.4	0.7	0.46	J152134.81+415418.8
1429820	211.7140	13.8063	66.8	-17.51	6.03	l	S	1.8±0.9	3.1	0.6	0.34	J140651.33+134822.7
1707313	140.4399	64.2579	18.7	-18.50	5.11	i	L	1.3±1.1	5.9	0.7	0.22	J092146.05+641527.9
1779654	146.6025	68.9572	56.7	-19.39	5.88	l	L	1.1±1.6	18.1	0.7	-0.07	J094624.58+685725.9
1818479	139.7722	31.1037	96.5	-18.91	5.15	l	S	3.0±0.7	7.5	0.8	-0.02	J091905.32+310613.5
1833424	180.2948	15.6263	88.1	-17.29	5.05	l	S	3.3±0.5	4.8	0.6	0.39	J120110.75+153734.5
1850708	171.8289	38.6642	81.8	-19.42	6.54	l	S	2.0±0.5	15.0	0.8	-0.03	J112718.94+383951.2
1881042	126.0615	34.3276	67.3	-17.77	7.27	l	L	3.3±0.5	7.7	0.7	-0.52	J082414.75+341939.4
1886162	126.5233	21.6676	56.2	-18.26	8.31	l	L	4.3±1.3	5.4	0.5	0.99	J082605.59+214003.2
1896022	198.3558	33.2902	61.5	-18.17	6.56	l	U	2.2±1.2	5.3	0.7	0.11	J131325.39+331724.9
1903932	127.0314	20.2621	56.8	-18.07	6.36	i	L	7.7±1.8	3.0	0.6	0.76	J082807.54+201543.6
1921468	183.1644	34.6894	82.2	-18.93	6.25	l	U	2.5±0.6	4.1	0.7	0.02	J121239.43+344121.8

Table 2
Continued

ID	α_{2000}	δ_{2000}	D (Mpc)	M_r	a/b	T^a	Warp	α_w (°)	r_w (kpc)	r_w/a	$\Sigma_7'^{\ b}$	SDSS name
1928213	177.5755	35.2541	82.3	-18.84	7.61	i	U	2.1±0.5	13.0	0.7	0.66	J115018.13+351514.6
1939722	191.7526	32.6516	19.7	-15.01	5.82	l	U	2.7±1.4	8.5	0.7	-0.17	J124700.64+323905.7
1942904	242.4618	20.1775	46.9	-17.55	7.50	i	L	1.8±0.6	8.7	0.7	-0.88	J160950.69+201039.9
1953502	196.8517	32.8627	68.3	-19.12	6.02	l	L	4.7±0.5	2.8	0.5	-0.11	J130724.41+325145.7
1964529	240.5228	18.6490	59.9	-16.95	5.36	l	S	2.5±0.9	0.9	0.6	0.20	J160205.30+183855.5
1982484	207.6103	28.1325	93.0	-18.11	5.04	l	L	2.2±1.5	2.5	0.5	-0.71	J160205.30+183855.5
1985756	223.9679	24.7195	64.2	-19.09	11.40	e	L	1.3±1.0	6.7	0.7	-0.20	J145552.30+244310.3
2171582	180.9570	29.7155	39.7	-18.02	5.97	l	L	1.7±1.1	10.6	0.7	0.64	J120349.68+294255.6
2202790	192.3490	29.3213	97.2	-18.46	6.71	l	L	4.0±0.5	3.3	0.6	0.11	J124923.76+291916.6
2214604	156.7547	28.6393	15.5	-16.88	7.21	l	S	3.0±0.2	1.5	0.6	0.34	J102701.12+283821.5
2225967	189.2015	27.5489	95.2	-19.90	5.40	i	L	5.3±0.5	9.5	0.5	0.85	J123648.36+273256.2
2239131	146.7248	23.0232	94.4	-19.34	6.31	i	L	8.0±1.8	10.7	0.6	0.16	J094653.94+230123.5
2239523	162.5315	26.4569	80.6	-18.40	7.52	i	S	13.4±2.7	3.3	0.5	0.97	J105007.55+262724.8
2248578	181.7636	25.7287	90.8	-18.29	5.66	l	L	4.3±0.3	4.5	0.7	1.31	J120703.25+254343.3
2254896	139.5827	17.7533	37.8	-17.52	7.35	l	U	5.2±0.5	10.9	0.7	-0.21	J091819.84+174511.8
2258076	150.3992	21.6075	79.9	-19.54	5.65	l	L	1.3±1.1	1.9	0.7	-0.17	J100135.81+213627.1
2260966	151.2469	21.5382	50.2	-17.82	5.96	l	L	3.5±1.0	13.6	0.8	-0.35	J100459.26+213217.6
2273079	130.8164	13.0858	26.1	-18.78	10.15	i	L	1.5±0.9	4.8	0.8	-0.18	J084315.92+130508.8
2288905	168.6218	22.4899	67.7	-19.17	5.22	l	L	1.0±1.4	6.0	0.6	-0.71	J111429.22+222923.5
2291338	172.8426	23.1149	36.4	-18.37	9.57	e	L	1.2±1.5	3.1	0.6	-0.01	J113122.21+230653.7
2298387	197.6779	21.3671	87.8	-18.26	6.44	l	S	4.2±1.5	7.2	0.6	0.28	J131042.68+212201.5
2301961	172.6127	21.6598	59.1	-16.18	6.36	l	L	8.3±1.9	3.5	0.6	-0.12	J113027.03+213935.3
2325122	196.3620	25.1912	92.3	-18.61	6.38	l	S	5.2±2.0	9.1	0.7	0.48	J130526.87+251128.1
2326526	179.1472	25.8219	63.3	-17.06	6.81	l	S	3.4±0.6	4.4	0.6	0.86	J115635.33+254918.6
2394504	181.8356	17.2616	86.7	-20.73	7.83	e	S	2.5±0.5	10.6	0.8	1.21	J120720.54+171541.8
2417256	201.1046	17.0930	94.5	-19.18	7.12	l	L	2.1±1.6	7.6	0.7	-0.03	J132425.09+170534.4
2484928	158.3921	17.7420	79.8	-18.40	6.66	l	L	2.5±0.2	5.1	0.7	-0.10	J103334.10+174431.0
2485995	144.1274	15.5488	55.2	-17.45	6.37	l	S	5.2±0.9	2.1	0.5	-0.49	J093630.57+153255.5
2496790	131.0914	9.5372	51.8	-17.80	6.93	l	U	5.1±2.0	5.4	0.7	-0.72	J084421.89+093214.1
3000043	123.4951	45.7455	5.6	-14.83	6.13	l	S	5.6±2.0	25.0	0.6	-0.25	J081358.76+454441.8
3124212	207.9264	51.0538	53.1	-16.77	5.13	l	L	3.2±0.8	1.6	0.6	-0.20	J135142.34+510313.7
3193135	183.9424	10.6992	16.7	-17.07	5.90	l	U	4.3±0.3	15.8	0.5	1.05	J121546.00+104203.3
3193804	123.4953	45.7418	5.6	-14.85	9.26	l	L	4.7±0.6	28.1	0.6	-0.26	J081358.87+454430.4
5000415	146.8942	-2.0347	16.4	-16.82	5.81	l	L	4.6±1.7	18.1	0.8	0.29	J094734.61-020204.8
216740	222.4420	60.3986	29.3	-18.01	6.75	l	L	1.1±2.6	18.3	0.6	0.29	J144946.09+602354.7
225578	125.6443	50.4409	94.6	-17.43	6.83	i	S	5.6±2.2	1.3	0.8	-0.47	J082234.56+502626.8
229197	178.8294	67.4026	85.8	-18.45	6.24	i	S	2.6±1.8	12.4	0.7	-0.41	J115519.05+672409.1
307903	312.4676	-7.0218	82.3	-20.44	6.61	i	S	4.5±0.2	21.0	0.6	-0.07	J204952.22-070118.4
446793	140.3143	3.1511	44.5	-18.68	10.35	i	L	2.0±1.2	5.4	0.5	0.02	J092115.42+030904.1
468199	118.7522	36.4632	78.5	-18.13	5.32	l	S	5.2±0.4	4.5	0.6	-0.44	J075500.52+362747.3
536922	234.2227	51.2887	77.1	-18.39	7.27	l	S	3.3±0.6	5.1	0.5	-0.80	J153653.45+511719.0
583667	254.3469	38.6715	26.9	-15.24	5.21	l	S	5.2±2.0	6.8	0.5	-0.90	J165723.38+384016.3
745567	340.2010	-1.1539	67.0	-18.22	5.22	l	S	4.8±1.5	5.4	0.6	-0.42	J224048.25-010913.6
1035522	139.9918	37.1913	28.1	-19.47	8.18	e	L	3.3±0.4	8.1	0.8	0.29	J091958.02+371128.5
1064688	167.5647	45.5712	96.6	-18.76	8.28	e	L	7.8±1.8	2.3	0.8	0.37	J111015.52+453416.3
1265804	211.0151	12.0047	94.4	-19.40	6.66	i	L	4.4±0.5	6.4	0.5	0.49	J140403.61+120016.8
1282369	186.4273	7.2166	16.7	-19.38	5.70	i	S	1.3±2.0	21.6	0.6	2.26	J122542.56+071259.9
1283153	211.0322	6.4859	96.9	-19.88	5.25	i	L	1.9±1.0	9.7	0.7	0.01	J140407.73+062909.2
1317761	190.5658	39.5647	71.8	-17.73	6.79	l	S	3.4±0.9	1.4	0.6	-0.07	J124215.76+393352.6
1353313	210.6480	9.1199	75.1	-18.91	6.73	e	S	8.2±1.3	4.4	0.5	1.58	J140235.51+090711.5
1363624	224.0505	5.7325	84.8	-17.52	5.09	l	U	6.3±2.6	2.5	0.7	-0.46	J145612.11+054357.1
1440094	213.8920	36.2266	36.8	-20.90	8.31	i	S	3.5±1.5	51.8	0.6	1.07	J141534.07+361335.6
1703250	135.4304	60.1574	41.1	-17.53	5.81	l	L	2.4±0.4	6.1	0.6	-0.52	J090143.33+600926.1
1834486	173.7846	15.9586	65.6	-18.61	5.99	l	S	3.5±1.1	6.2	0.6	-0.12	J113508.28+155731.0
1855974	160.9994	37.8231	91.2	-17.70	7.60	l	S	4.2±0.3	4.6	0.6	0.62	J104359.84+374923.1
1918746	201.6311	33.1836	93.0	-17.69	5.51	l	L	0.9±0.4	4.5	0.6	0.35	J132631.49+331059.9
1966772	237.1725	21.8698	28.5	-18.39	27.79	e	S	2.3±0.2	11.8	0.8	-0.25	J154841.40+215211.1
2017792	214.1967	23.0025	59.7	-19.32	5.31	i	L	1.8±0.8	6.0	0.8	0.23	J141647.20+230008.8
2286160	178.1060	22.7034	92.8	-17.93	5.61	l	L	5.1±0.1	5.5	0.5	0.44	J115225.41+224212.3

Table 2
Continued

ID	α_{2000}	δ_{2000}	D (Mpc)	M_r	a/b	T[a]	Warp	α_w (°)	r_w (kpc)	r_w/a	Σ_7' [b]	SDSS name
2289904	209.3561	21.3894	36.4	-17.66	6.49	l	S	9.9±2.2	0.9	0.5	-0.46	J135725.47+212321.7
2357338	182.6542	18.8287	30.2	-18.40	7.12	l	S	4.6±0.5	4.5	0.7	0.21	J121037.02+184943.4
5000164	190.6053	-6.9711	35.5	-20.50	5.67	i	S	6.4±1.2	16.3	0.7	0.36	J124225.26-065815.9
448589	142.9406	3.7287	40.4	-16.58	6.93	l	S	7.4±1.7	7.5	0.7	-0.02	J093145.75+034342.8
834511	121.1463	35.9977	72.7	-18.05	5.83	l	U	1.6±1.6	5.9	0.7	-0.17	J080435.11+355952.
1941055	204.2545	31.7665	38.1	-17.70	6.77	l	U	1.7±0.4	14.8	0.6	-0.80	J133701.07+314559.4
1985065	203.9637	29.2139	82.6	-17.95	5.25	l	U	3.9±0.5	1.7	0.7	-0.81	J133551.27+291249.9
38349	191.9708	-1.1858	91.1	-19.68	8.56	i	L	2.0±0.1	11.9	0.7	-0.12	J124752.98-011109.0
78895	149.7076	0.8367	48.2	-17.28	5.36	l	L	2.3±0.3	1.1	0.6	-0.62	J095849.83+005012.1
163161	195.2783	-3.3764	36.5	-16.95	5.35	l	L	2.2±1.1	8.2	0.9	-0.42	J130106.81-032234.2
216387	153.0505	62.0971	39.2	-16.56	5.27	l	S	2.9±1.4	8.9	0.5	-0.18	J101211.89+620549.7
265279	185.8749	2.0081	21.9	-15.40	5.92	l	L	2.2±1.1	8.9	0.8	1.00	J122329.97+020029.0
382320	5.8991	15.2353	73.5	-17.80	6.07	l	S	1.9±1.0	6.2	0.6	0.38	J002335.78+151407.1
450272	149.3189	4.5270	26.3	-18.05	5.98	i	L	1.3±0.7	13.4	0.7	0.15	J095716.52+043137.0
470092	115.8871	31.5353	48.0	-17.23	6.77	l	L	3.2±0.9	3.7	0.7	0.16	J074332.90+313206.9
522028	187.2180	4.2931	54.0	-18.79	8.93	i	L	1.7±0.9	19.9	0.7	0.33	J122852.29+041734.9
596529	214.7822	5.3838	96.2	-18.40	6.45	l	L	3.2±0.7	2.5	0.6	0.06	J141907.71+052301.2
598385	236.2062	3.9564	46.3	-17.53	5.65	l	L	2.0±0.2	2.3	0.4	-0.28	J154449.46+035722.8
727536	345.0157	15.0196	99.7	-18.64	8.71	i	L	2.8±0.6	1.5	0.8	0.16	J230003.75+150110.6
744805	329.0578	-1.1620	66.7	-17.74	5.23	l	L	3.9±1.2	2.9	0.6	-0.19	J215613.86-010943.3
761257	35.4633	-0.9627	96.1	-17.65	5.32	l	U	4.2±1.6	1.7	0.6	-0.40	J022151.19-005745.3
763545	35.6251	-0.6175	22.1	-15.18	5.76	l	L	1.2±0.6	8.7	0.7	-0.19	J022229.88-003704.1
823112	119.3238	31.4701	68.2	-18.07	5.58	l	S	1.9±0.5	3.5	0.7	-0.00	J075717.69+312812.4
827691	119.2422	34.5568	53.8	-16.63	6.11	e	L	1.6±0.5	1.9	0.7	-0.47	J075658.12+343324.6
830406	119.3970	32.3491	54.4	-16.76	5.98	l	L	1.6±0.5	2.9	0.7	-0.14	J075735.27+322056.6
846063	183.9488	52.1258	43.7	-16.85	6.46	l	L	1.2±0.2	9.8	0.6	-0.44	J121547.71+520732.5
866803	133.6441	40.0270	93.6	-19.09	5.79	l	L	1.5±0.8	5.7	0.8	0.27	J085434.58+400137.1
870648	183.8840	51.9132	51.1	-17.71	5.25	l	L	1.3±0.6	7.3	0.9	-0.43	J121532.15+515447.1
910935	133.3864	4.7824	80.3	-18.79	5.30	i	L	1.1±0.5	6.6	0.6	-1.27	J085332.73+044656.7
926455	177.5514	6.9985	77.4	-19.56	9.98	l	S	1.7±0.9	8.4	0.8	0.80	J115012.33+065954.5
932346	153.2049	7.1038	18.1	-15.97	5.35	l	L	2.2±0.3	7.3	0.6	0.00	J101249.18+070613.6
959193	185.8213	11.3679	16.7	-18.54	6.11	l	L	2.3±1.1	35.0	0.6	1.30	J122316.82+112159.7
980703	216.8062	50.5624	50.8	-18.08	6.02	l	U	2.2±1.1	8.3	0.8	-0.70	J142713.49+503344.6
1006813	236.0292	47.2946	78.4	-18.36	7.55	l	L	3.3±1.7	13.2	0.8	0.04	J154407.10+471740.7
1057873	168.0644	8.6288	41.6	-16.74	5.42	l	S	2.8±0.6	8.8	0.7	-0.78	J111215.43+083743.6
1076121	156.1553	11.9080	29.9	-16.46	5.51	l	L	1.8±0.9	7.6	0.6	0.11	J102437.26+115428.9
1089277	150.4059	39.6272	90.0	-20.12	7.00	i	L	1.1±0.5	22.9	0.8	-0.26	J100137.39+393738.2
1090155	126.4483	28.1181	27.7	-17.77	5.27	l	L	2.9±1.4	21.6	0.8	0.49	J082547.60+280705.2
1124474	168.8710	13.6087	95.5	-19.37	5.06	l	L	3.9±1.9	7.4	0.7	-1.13	J111529.05+133631.2
1130975	151.9881	13.2274	34.3	-17.18	6.14	l	S	3.8±1.9	8.0	0.7	0.27	J100757.11+131338.6
1158913	141.4277	34.8565	62.5	-17.78	6.16	l	L	1.6±0.8	1.7	0.7	0.29	J092542.64+345123.5
1163286	218.4393	44.0822	39.2	-16.55	5.73	l	L	3.4±1.7	3.2	0.6	-0.10	J143345.42+440455.8
1168388	163.5453	44.6243	95.2	-19.65	5.06	i	L	1.5±0.7	13.1	0.8	-0.24	J105410.86+443727.2
1200519	201.1463	57.0528	81.6	-17.37	5.02	l	S	3.3±1.1	2.8	0.6	-1.00	J132435.10+570309.7
1221667	176.5375	12.8796	41.4	-16.24	5.14	l	L	2.4±1.2	1.6	0.8	0.81	J114608.96+125246.5
1262738	210.9090	11.5735	78.1	-18.14	5.06	l	L	1.4±0.7	6.9	0.8	-0.15	J140338.15+113424.5
1299465	194.8854	42.7590	93.3	-18.40	5.77	l	U	2.4±0.4	3.3	0.6	-0.45	J125932.49+424532.2
1301738	209.5367	10.2734	88.4	-18.26	5.56	l	L	3.0±0.3	7.7	0.8	0.94	J135808.78+101624.3
1313540	172.5385	38.6204	81.6	-19.52	5.15	l	S	4.0±2.0	11.0	0.7	0.07	J113009.25+383713.6
1324090	248.7307	20.5788	57.9	-18.76	6.42	l	L	1.3±0.7	5.8	0.7	-0.54	J163455.36+203443.7
1335657	219.6950	7.6174	72.1	-18.43	6.73	l	L	2.9±1.4	6.3	0.8	-1.29	J143846.80+073702.8
1429361	241.2452	8.4537	68.7	-17.43	6.28	l	S	4.0±1.2	0.9	0.6	-0.28	J160458.84+082713.3
1770037	21.2028	1.0363	64.9	-16.67	7.15	l	S	3.5±1.7	1.4	0.7	-0.09	J012448.57+010212.9
1778252	146.0094	68.3703	56.7	-17.70	5.28	l	L	4.6±2.3	4.2	0.8	-0.06	J094402.25+682213.0
1860904	200.5334	35.3931	77.4	-17.61	5.49	l	L	2.9±1.4	4.1	0.6	0.21	J132208.02+352335.1
1899887	170.4916	34.9486	24.7	-16.77	5.72	l	L	1.2±0.6	2.4	0.7	0.48	J112157.96+345654.8
1944554	180.3222	31.2780	89.7	-18.69	6.89	l	S	4.1±2.0	1.0	0.7	0.17	J120117.33+311640.8
1952138	213.0679	29.9074	56.5	-17.62	5.53	l	L	1.4±1.4	1.5	0.7	-0.45	J141216.27+295426.7
1971273	213.7546	26.7169	67.9	-18.25	5.06	i	L	2.6±1.3	1.1	0.7	-0.27	J141501.09+264300.6

Table 2
Continued

ID	α_{2000}	δ_{2000}	D (Mpc)	M_r	a/b	T^a	Warp	α_w (°)	r_w (kpc)	r_w/a	Σ_7' [b]	SDSS name
1998392	222.4152	23.5611	69.0	-18.04	6.18	l	L	1.5±0.7	7.8	0.8	-0.15	J144939.62+233339.4
2173678	156.9336	27.1435	84.6	-19.28	5.29	i	L	1.1±0.5	9.6	0.7	0.15	J102744.06+270836.7
2221413	188.9226	26.2858	81.4	-18.89	6.47	l	L	1.9±0.9	8.0	0.7	1.49	J123541.42+261708.9
2236134	170.7239	26.6049	77.3	-17.91	5.71	l	S	1.6±0.8	9.3	0.7	0.40	J112253.72+263617.6
2259887	150.3946	19.9666	63.1	-17.55	5.99	l	L	1.0±0.3	4.9	0.5	-0.85	J100134.69+195759.5
2264934	173.8913	24.9626	89.5	-19.00	6.41	l	L	2.5±0.2	6.0	0.7	0.42	J113533.90+245745.2
2277411	221.9957	17.4031	80.9	-18.03	5.70	l	S	2.4±1.2	4.3	0.6	-0.27	J144758.95+172411.1
2318919	168.2104	23.2566	82.0	-19.66	5.12	l	L	2.1±1.0	9.6	0.8	1.04	J111250.48+231523.8
2342952	200.7092	19.6908	87.3	-19.36	5.64	i	L	1.3±0.7	12.6	0.8	0.24	J132250.20+194126.9
2354400	173.4796	19.3600	47.4	-18.12	11.50	i	L	1.3±0.6	4.7	0.7	0.29	J113355.11+192136.0
2392445	173.7300	16.1160	69.8	-19.08	6.89	l	L	2.9±1.4	8.9	0.8	0.13	J113455.19+160657.6
2393339	175.8448	16.4854	84.5	-20.44	6.41	i	L	1.2±0.6	15.3	0.8	0.20	J114322.74+162907.4
2493429	151.1229	14.7692	90.4	-19.11	5.34	i	L	3.7±1.9	5.3	0.6	-0.02	J100429.63+144549.6
5000166	191.0795	-5.5368	33.4	-18.20	7.09	l	L	2.0±1.0	11.3	0.7	0.32	J124419.07-053212.5
9000014	44.6963	75.7447	35.2	-19.34	9.49	l	L	1.1±0.6	37.1	0.7	-1.25	J025847.10+754440.7

[a] Labels 'e', 'i', and 'l' denote early, intermediate, and late type spirals, respectively.
[b] Σ_7' is defined as $\log(\Sigma_7/\bar{\Sigma}_7)$

Park (2006). They found that the mean warp radius r_w is close to R_{25} ($r_w \approx 0.9R_{25}$) and is about $0.7R_{opt}$ where R_{opt} is the radius of the visible disk which is measured at the isophotes ~ 4 mag fainter than the sky brightness (Ann & Park 2006). While warp angles are independent of the galaxy distance, the warp radius (r_w), as measured in units of kpc, depends on the galaxy distance. To avoid the effect of errors associated with the distance of a galaxy, warp radius is usually expressed in units of a characteristic length, such as R_{25} (Ann & Park 2006) and disk scale length (Saha et al. 2009). Here, we express it in units of the major axis length (a). Since we measured a at $\mu_r \sim 26.5$ mag arcsec^{-2}, which is at least ~ 0.5 mag arcsec^{-2} deeper than the photometry of Ann & Park (2006), a is slightly larger than R_{opt} of Ann & Park (2006). The mean radius of 192 warped galaxies is 8.2 ± 7.2 kpc with the mean r_w/a of 0.67 ± 0.08. Some galaxies have r_w as small as half of a, but, as shown in Figure 6, the majority of warped disks have a warp radius that is larger than $0.6a$; the frequency distribution of the r_w/a peaks at 0.65. In this study, we used the mean r_w for S- and U-shaped warps. We confirm the anti-correlation between r_w/R_{opt} and α_w (Figure 10 of Ann & Park 2006), i.e., warp angles are proportional to the inverse of r_w/a.

3.4. Warp Asymmetry

Although some S-shaped warps look very symmetric, most disks have asymmetric warps. The asymmetry is more pronounced in conspicuous warps (Reshetnikov et al. 2016). Asymmetric S-shaped warps could be formed by a variety of causes. Sanchez-Salcedo (2006) showed that asymmetry is a general feature of accretion driven warps and Kim et al. (2014) showed that fly-by encounters frequently give rise to asymmetric S-shaped warps. The L-shaped warp is an extreme case of an asymmetric warp. The asymmetry in the warp radius is affected by the lopsidedness of the galaxies that is observed in

$\sim 30\%$ of spiral galaxies (Rix & Zaritsky (1995; Zaritsky & Rix 1997; Kornreich 1998) whereas the asymmetry in the warp angles seems to be related to the intrinsic properties of warps (Garcia-Ruiz et al. 2002). Jeon et al. (2009) showed that there is no S-shaped warp formed by the torques from the misaligned halo.

There are two ways of defining the asymmetry in the warp angle. One is defined as the simple difference between the warp angles in the east and west sides of the disk, i.e., $A_w = |\alpha_{w,e} - \alpha_{w,w}|$ (Garcia-Ruiz et al. 2002) where $\alpha_{w,e}$ and $\alpha_{w,w}$ are the warp angles in the east and west sides of the disk, respectively. The other is defined as $|\alpha_{w,e} - \alpha_{w,w}|/(\alpha_{w,e} + \alpha_{w,w})$ (Castro-Rodriguez et al. 2002). We used the definition of Garcia-Ruiz et al. (2002).

Figure 7 shows a plot of the warp asymmetry A_w as a function of α_w for all U-shaped and S-shaped warps. As shown in Figure 7, there is a tight correlation between the warp asymmetry and warp angle. There is no appreciable difference between the U-shaped warps and S-shaped warps. Similar relations were reported by Garcia-Ruiz et al. (2002) and Ann & Park (2006) but the present data show much stronger correlation than those of Garcia-Ruiz et al. (2002) and Ann & Park (2006). The reason for the tighter correlation of the present study is due to the small measurement errors in warp angles, thanks to digital tools rather than a ruler on the paper. The largest asymmetries in Figure 7 are observed in galaxies located in the high density regions where the nearest neighbor galaxies are very close. This agrees with the finding of Ann & Park (2006) who showed that the largest asymmetries in their data were found in the galaxies that have companion galaxies.

3.5. Morphological Types of Warped Galaxies

We classified the morphological types of 340 edge-on galaxies by visual inspection of the color images from the SDSS DR7. Only two galaxies are classified as
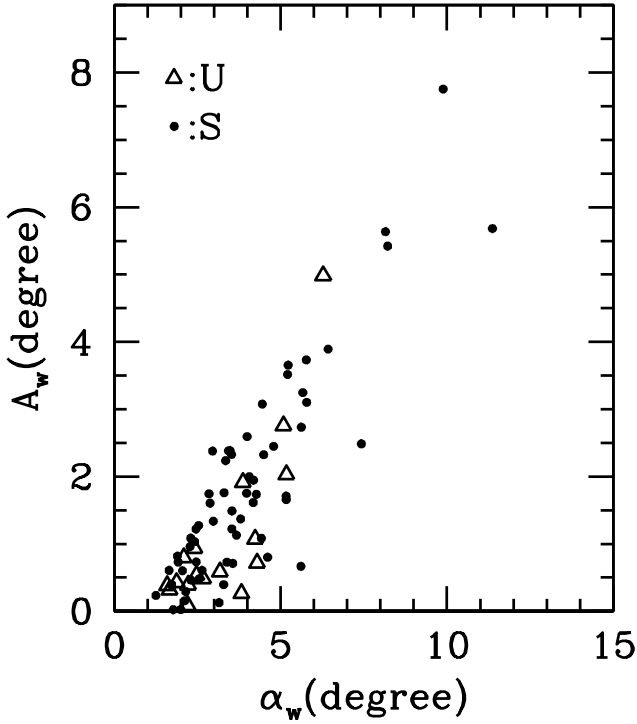
Figure 7. Warp asymmetry versus warp angle. The U-shaped warps are indicated by the open triangles and the S-shaped warps are represented by filled circles.
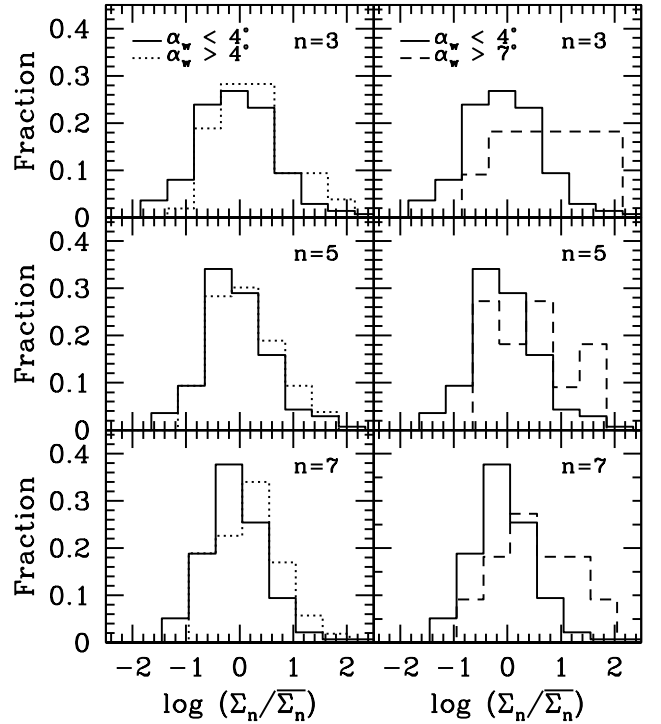

Figure 8. The $\Sigma_n/\bar{\Sigma}_n$ distribution of warped galaxies. The strong warps ($\alpha_w > 4°$) and the highly strong warps ($\alpha_w > 7°$) are plotted in the left panel and in the right panel, respectively, with the weak warps ($\alpha_w < 4°$) which are indicated by the solid line. The strong warps and the highly strong warps are plotted by dotted line and short-dashed line, respectively.

lenticular galaxies (S0) and the rest are spiral galaxies. We grouped the morphological types of spiral galaxies into three broad types of stages: early type (e), intermediate type (i), and late type (l). The Hubble stages of the early type spirals consist of 0/a, a, and ab, while those of the intermediate type spirals are b, bc, and c. Other Hubble stages belong to the late type spirals. Table 1 summarizes the frequency distribution of 340 edge-on galaxies sorted by morphological type and warp type. As shown in Table 1, most of the sample galaxies are late type spirals ($\sim 73\%$). The middle type spirals are $\sim 23\%$. The paucity of S0 galaxies in the present sample is due to the size and axis ratio distributions of S0 galaxies, which are different from the spiral galaxies (Ann et al. 2015). In the local universe ($z < 0.01$), most S0 galaxies have axis ratios that are smaller than $a/b = 5$. There are no warped S0 galaxies in the present sample. The absence of warped S0 galaxies was reported by Sanchez-Saavedra et al. (2003) who thought that the lack of gas in S0 galaxies is the cause for the absence of warped S0 galaxies in their sample.

The fraction of early type spirals is much smaller than the fraction of early type spirals given in the Catalog of Visually Classified Galaxies (Ann et al. 2015), which shows that there are similar fractions for e, i, and l. The small fraction of early type spirals ($\sim 3\%$) in the present sample is due to the paucity of early type spirals that have large axis ratios. The size and axis ratio distributions of lenticular and spiral galaxies are thought to be closely related to the structure evolution of these

galaxies driven by internal and external causes.

The L-shaped warps comprise $\sim 55\%$ of the early type spirals, which is about double the number of S-shaped warps. The dominance of L-shaped warps compared with U- and S-shaped warps in early type spirals is understandable if we consider that L-shaped warps are the most abundant types of warps. The paucity of galaxies with no detectable warp in the early type spirals is different from the even distribution of warped galaxies along the Hubble sequence (Sanchez-Saavedra et al. 2003). We conjecture that there exist favorable conditions for warp formation in the early type spirals. One of the favorable conditions is the large bulge and massive dark halo of the early type spirals that can drive gravitational torques if they are misaligned with the disk rotation axis. The environment of the early type spirals also seems to provide favorable conditions for disk warping via tidal interactione because they are likely to be located in high density regions (Dressler 1980). While the L-shaped warps are the most dominant warp types in the early type spirals, they contribute only $\sim 30\%$ of the late type spirals. The most dominant ones are the galaxies with no detectable warps which comprise $\sim 43\%$ of the late type spirals. The fraction of no detectable warps in the late type spirals is about four times larger than that of the early type spirals. However, the largest fraction of spiral galaxies
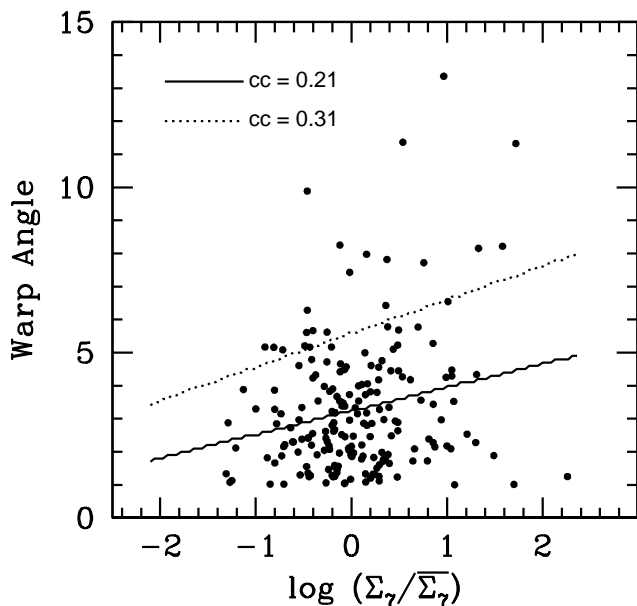
Figure 9. Correlation between α_w and $\Sigma_7/\bar{\Sigma}_7$ for galaxies with warped disks. The sold line is the least squares solutions for all warped galaxies and the cc is a correlation coefficient. The dotted line represents the least-squares solutions for the strong warps ($\alpha_w > 4°$) only.
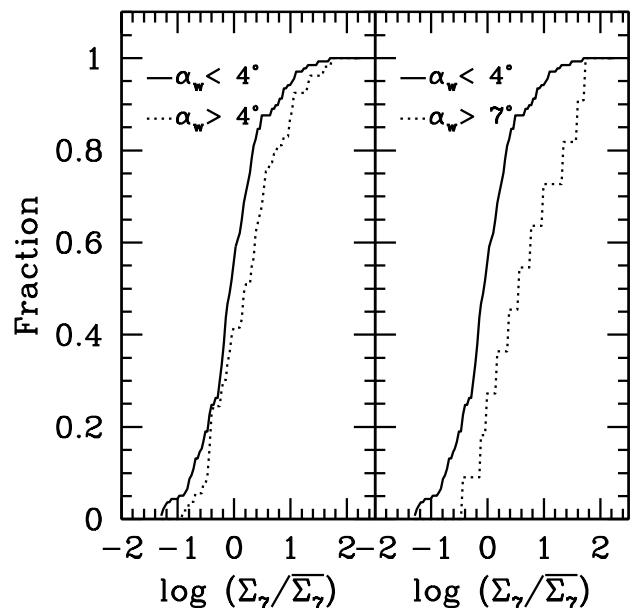

Figure 10. Cumulative distribution of $\Sigma_7/\bar{\Sigma}_7$, for strong warps (in the upper panels) and highly strong warps (lower panels). The weak warps are used as the comparison sample (solid line).

with no detectable warps occurs in intermediate type spirals where the fraction is $\sim 50\%$. Owing to the large fraction of no detectable warps in the intermediate type spirals, U-shaped and S-shaped warps comprise only 2.5% and 14% of the intermediate type spirals. The fraction of L-shaped warps in the intermediate type spirals is similar to that of late type spirals.

4. ENVIRONMENTAL DEPENDENCE OF WARP AMPLITUDE

4.1. Derivation of Environment Measures

We used the local background density as a measure of the galaxy environment. While there are several ways to define local background density of galaxies (Muldrew et al. 2012), we employed the local background density derived from the projected distances to the nth nearest neighbor galaxies, Σ_n. There are several values of n in literature but we used $n=7$ after some trials with other values of n. Small values of n give higher density resolutions than the large values of n. The proper choice of n is as important as the other constraints required in the nth nearest neighbor method, the linking velocity ΔV^* and the limiting magnitude M_r^* to define neighbor galaxies.

It is not a trivial matter to define neighbor galaxies because the distances of the galaxies are not accurate enough to determine their three-dimensional spatial distributions. This is due to the peculiar motions of galaxies that are substantial fractions of the Hubble flow in the nearby universe. The most widely used practice of searching for neighboring galaxies is to use projected distance with a constraint on the velocity difference (ΔV) between a target galaxy and its neighbor

galaxies. For small systems, such as galactic satellite systems and small groups of galaxies, ΔV is usually smaller than $\sim 500\,\mathrm{km\,s^{-1}}$, while ΔV of cluster galaxies may exceed $1000\,\mathrm{km\,s^{-1}}$ (Choi & Ann 2011). We adopt the value $500\,\mathrm{km\,s^{-1}}$ for the linking velocity, i.e., the maximum velocity difference between a target galaxy and its neighbor galaxies, ΔV^* by considering that the rms peculiar velocities of galaxies is $\sim 500\,\mathrm{km\,s^{-1}}$ (Peebles 1979, 1987). In searching for neighbors, we also need to constrain the limiting luminosity of the neighbor galaxies (M^*). This was because the present sample is a flux-limited sample due to the constraint on the apparent magnitudes of the target galaxies of the spectroscopic observations in the SDSS. We took M^* as -17.23, which corresponded to the absolute magnitude of a galaxy with an apparent r-band magnitude of 17.77 at $z = 0.025$. By adopting $M^* = -17.23$, we made a volume-limited sample.

We calculated Σ_n using the following equation,

$$\Sigma_n = \frac{n}{\pi r_{p,n}{}^2} \qquad (1)$$

where $r_{p,n}$ is the projected distance to the nth nearest neighbor galaxy. We normalized Σ_n using the mean local background density ($\bar{\Sigma}_n$) of the SDSS galaxies with $z < 0.025$ using the SDSS DR7 (Abazajian et al. 2009).

We present the $\Sigma_7/\bar{\Sigma}_7$ together with the warp parameters of 192 warped galaxies in Table 2. We also give the coordinates and the names of the galaxies, KIAS VAGC ID in the first column and SDSS ID in the last column, for an easy identification of the galaxies. The quoted errors of warp angles are derived from multiple measurements.
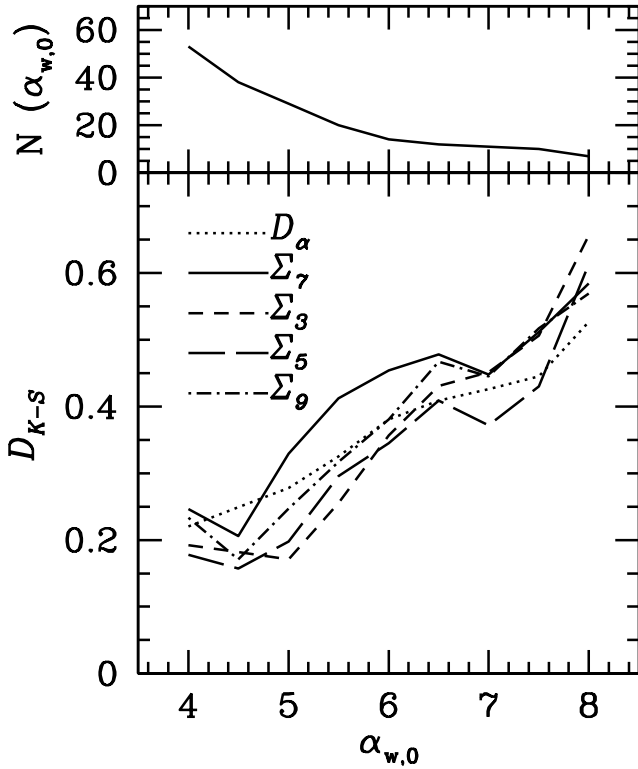
Figure 11. Number of sample galaxies (upper panel) and the D_{K-S} compared with the K-S D_α (lower panel) for Σ_n as a function of the minimum warp angle $\alpha_{w,0}$. The dotted line (D_α) is calculated by assuming a significance level of $\alpha = 0.05$.

4.2. Frequency Distribution of the Local Background Density

Figure 8 shows the frequency distributions of the Σ_7 for 192 warped galaxies along with those for Σ_3 and Σ_5. We examined weak warps ($\alpha_w < 4°$), strong warps ($\alpha_w > 4°$), and highly strong warps ($\alpha_w > 7°$). There are considerable differences between the highly strong warps and the weak warps for Σ_7 as well as Σ_3 and Σ_5 while there is no significant difference between the strong and weak warps. The highly strong warps are likely to be found in dense regions where the tidal strength from neighbor galaxies is strong. These preferences are indicated by the large excess of highly strong warps at $\log (\Sigma_n/\bar{\Sigma}_n) > 1$. There is not much difference among the local background densities derived from $n = 3$, $n = 5$, and $n = 7$. However, the K-S test shows that Σ_7 distinguishes the strong warps from the weak warps more clearly.

4.3. Correlation between Environment Measures and Warp Amplitude

Figure 9 shows the correlations between α_w and Σ_7 for warped galaxies. As shown by the regression lines of the least-square solutions, the correlations are not strong. Moreover, if we consider the weak warps only, i.e., $\alpha_w < 4°$, there is virtually no correlation between the warp angle the local background density. This is

the reason why there has been conflicting argument for the relationship between the warp frequency and the environment of galaxies (Reshetnikov & Combes 1998; Garcia-Ruiz et al. 2002). There is a lot of scatter with larger deviations for the highly strong warps. The weak correlations lead to small Pearson correlation coefficients (cc) given in the upper part of each panel in Figure 9. However, if we consider only the strong warps ($\alpha > 4°$), the correlations become slightly tighter with cc = 0.31.

The large scatter and the weak correlations between the warp angle and the local background density seem to be associated with the diversity of warp-driving mechanisms. Some mechanisms depend on the galaxy environment, while others do not. One plausible mechanism that does not depend on the environment of a galaxy is the gravitational torque from a misaligned halo (Debattista & Sellwood 1999; Ideta et al. 2000; Jeon et al. 2009) or accreting intergalactic medium (Ostriker & Binney 1989; Jiang & Binney 1999; Lopez-Corredoira et al. 2002; Shen & Sellwood 2006). Other mechanisms, such as encounters with fly-by satellites and subhalos (Quinn, Hernquist, & Fullagar 1993; Huang & Carlberg 1997; Kim et al. 2014; Gomez 2016), do not directly relate to Σ_7 because they are not taken into account in the derivation of the local background density. Since the misaligned halos can easily drive strong symmetric S-shaped warps (Jeon et al. 2009), some highly strong warps that deviate much from the regression line might be caused by the gravitational torque from the misaligned halo.

The correlations between α_w and Σ_7 are affected by the errors (σ_w) in the derived α_w. Especially in case of highly strong warps, the measurement errors lead to large deviations from the regression lines. To reduce the effect of measurement errors, we measured the relevant lengths at least twice for the whole sample of galaxies and estimated more than three times for galaxies with highly strong warps.

4.4. K-S Test

To quantify the statistical significance of the differences in the frequency distributions of the local background density (Figure 8), we applied the Kolmogorov-Smirnov (K-S) test to the local background density after converting the frequency distributions to cumulative distributions. Figure 10 shows the cumulative distributions of the local background density for the strong ($\alpha_w > 4°$) and highly strong ($\alpha_w > 7°$) warps compared with the cumulative distributions of the weak warps. The observed K-S statistic D_{K-S} is defined as the maximum difference in the cumulative distributions of the program sample and the comparison sample. As expected from the frequency distributions of the local background density of the warped galaxies (Figure 8), the sample of highly strong warps showed a large D_{K-S}.

The K-S test uses the K-S statistic D_α where α is a significance level of the K-S test to test the null hypothesis that the two samples are drawn from the same population. We rejected the null hypothesis if

$D_{K-S} \geq D_\alpha$. The K-S statistic D_α depends on the size of the two data sets, n_1 and n_2, and a constant, $C(\alpha)$ that depends on α (Wall & Jenkins 2003). That is,

$$D_\alpha = c(\alpha)\sqrt{(n_1 + n_2)/n_1 n_2} \qquad (2)$$

where $C(\alpha)$ is 1.22, 1.36, and 1.48, respectively for $\alpha = 0.10$, $\alpha = 0.05$, and $\alpha = 0.025$. We adopted $\alpha = 0.05$ in the K-S test.

Since the K-S statistic D_α depends on the number of the two samples and their cumulative distributions from which D_{K-S} is defined, we examined the K-S test for subsamples defined by varying the minimum warp angle ($\alpha_{w,0}$) for warped galaxies to be selected. Figure 11 shows the result of the K-S test of Σ_n for the subsamples selected by $\alpha_{w,0}$. We examined Σ_n with n=3, 5, 7, and 9. Here, we use the weakly warped galaxies as the comparison sample. The number of galaxies in the subsample selected is shown in the upper panel of the figure. Note that the number of sample galaxies rapidly decreases with increasing $\alpha_{w,0}$. It is evident that the local background density of the strongly warped galaxies, defined by Σ_7, is significantly different from that of the weakly warped galaxies. For the subsamples selected by $\alpha_{w,0} > 6.5°$, Σ_3 and Σ_9 of strongly warped galaxies are different from those of weakly weakly warped galaxies. In case of Σ_5, only extremely strong warps with $\alpha_w \gtrsim 8°$ are distinguished from the weak warps.

5. DISCUSSION AND CONCLUSIONS

We have explored the environmental dependence of warp phenomena in disk galaxies using 192 warped galaxies which have detectable warp angles among the 340 edge-on galaxies with $a/b > 5$ selected from the KIAS VAGC (Choi et al. 2010). We use the local background density (Σ_n) as a measure of environment to see whether the warp phenomena depend on the local background density. We consider the warp angle (α_w) to be a representative measure of the warp amplitude. We determined α_w from color images using the SDSS Navigate Tool together with the calibrated isophotal maps. Since measurement errors are not negligible in most cases, we measured α_w at least twice to avoid spurious results. The mean measurement error σ_w is $\sim 1.0°$, but it could be as large as $\sim 3°$. The large errors are mostly associated with the uncertainties in the mean major axis selected by visual inspection of the color images of galaxies. Some galaxies show a curved major axis, which leads to large errors in warp angles.

As indicated by the correlation coefficient of ~ 0.20, the correlations between the local background density and warp amplitude are quite weak. The weak correlations are due to the dominance of weakly warped galaxies ($\alpha_w < 4°$), which are assumed to be formed by a variety of mechanisms, including internal causes, such as bending modes (Lyndenn-Bell 1965; Spark & Casertano 1988; Revaz & Pfenniger 2004), gravitational torque from the misaligned halo (Debattista & Sellwood 1999; Ideta et al. 2000; Jeon et al. 2009), or precessing bar (Sanchez-Martin, Romero-Gomez & Masdemont 2016). Large measurement errors also contribute

to the weak correlations. Nevertheless, there is a clear trend that indicate that the strong warps are likely to be found in high density regions, which provide favorable conditions for strong tidal strength. The K-S test shows that the Σ_7 of strongly warped galaxies is significantly different from that of the weakly warped galaxies. However, if we exclude the highly strong warps ($\alpha_w > 7°$), there is no significant difference between the strongly warped and weakly warped galaxies.

The correlations between the local background density and warp amplitude can be affected by the constraints on the neighbor galaxies. In this study, we used two parameters to select neighbor galaxies: ΔV^* and M_r^*. The former is the upper limit of the recession velocity difference (ΔV) between a target galaxy and its neighbor galaxies, while the latter is the lower limit of the galaxy luminosity (M_r) for neighbor galaxies. The constraint on ΔV is required because we use the galaxy distances derived from the redshifts of galaxies that are affected by the galaxy peculiar motions. The constraint on M_r is required by the observational limit of the sample galaxies. We adopted $M_r^* = -17.23$ to make the sample of the background galaxies a volume-limited sample since it is the absolute magnitude of a galaxy at $z = 0.025$ with $r = 17.77$, which is the limiting magnitude of the target galaxies in the SDSS spectroscopic observations. There seems to be no better choice of M_r^* than that adopted here for the present sample.

The constraint on ΔV^* is of a great importance for the derivation of environmental measures. It should reflect the peculiar velocities of galaxies in the local universe. However, there have been many investigations which report different values of the rms peculiar velocities, ranging from ~ 50 kms^{-1} to ~ 1000 kms^{-1} (Karachentsev 1971; Fesenko 1973; Davis et al. 1978; Peebles 1979; Tsvetkov 1981; Bean et al. 1983; Dreassler et al. 1987; Lynden-Bell et al. 1988; Calzetti & Giavalisco 1993; Giovanelli et al. 1996; Raychaudhury & Saslaw 1996; Hawkins et al. 2003). The adopted value of $\Delta V^* = 500$ kms^{-1} seems to be reasonable because the sample galaxies are located in a variety of environments. The effect of ΔV^* on the correlation between the local background density Σ_n and disk morphology as represented by Hubble type, spiral arm class, and bar type was examined by Ann (2014) who showed that $\Delta V^* = 500$ kms^{-1} had better correlation between the Σ_n and disk morphology.

Proper choice of n, which is the number of neighbor galaxies to be searched for, is also important because it constrains the resolution or smoothing length of the local background density. There are several choices for n in the literature (Muldrew et al. 2012). Ann (2014) explored the effect of n and ΔV^* on Σ_n in connection with the disk morphology of spiral galaxies and found that the local background density with $n = 3$ and $\delta V^* = 500$ kms^{-1} resulted in the best correlations with the Hubble types and arm classes. We examined the case for $n = 3$, $n = 5$, and $n = 9$ together with $n = 7$ and found that other values of n give similar, but slightly weaker, correlations than $n = 7$.

There is an inherent limitation in the present study due to the subjectivity in the parameter determination. Most of the large measurement errors are associated with uncertainties in the mean major axis, which is defined by a visual inspection of the images using image display tools. Some of the galaxies have a curved major axis of which the position angle is difficult to be defined. They contribute to the weak correlation between the environment measures and α_w. However, we think that the conclusion of the present study is not severely affected by these errors.

REFERENCES

Abazajian, K. N. et al. 2009, The Seventh Data Release of the Sloan Digital Sky Survey, ApJS, 182, 543

Ann, H. B., & Lee, H.-R. 2013, Spiral Arm Morphology of Nearby Galaxies, JKAS, 46, 141

Ann, H. B. 2014, Environment Dependence of Disk Morphology of Spiral Galaxies, JKAS, 47, 1

Ann, H. B., Seo, M., & Ha, D. K. 2015, A Catalog of Visually Classified Galaxies in the Local ($z < 0.01$) Universe, ApJS, 217, 27

Ann, H. B., & Park, J.-C. 2006, Warped Disks in Spiral Galaxies, New Astron., 11, 293

Aumer, M., White S. D. M., Naab T., & Scannapieco, C. 2013, Towards a More Realistic Population of Bright Spiral Galaxies in Cosmological Simulations, MNRAS, 434, 3142

Bailin, J., & Steinmetz, M. 2005, Internal and External Alignment of the Shapes and Angular Momenta of ΛCDM Halos, ApJ, 627, 647

Bailin, J., & Steinmetz, M. 2005, in Near-Fields Cosmology with Dwarf Elliptical Galaxies, ed. Jeren, H., & Binggeli, B. (Cambridge: Cambridge University Press), 207

Battaner, E., Florido, E., & Sanchez-Saavedra, M. L. 1990, Intergalactic Magnetic Field and Galactic Warps, A&A, 236, 1

Battaner, E., & Jimenez-Vicente, J. 1998, A Simple Model of Magnetically Induced Warps, A&A, 332, 809

Bean, A. J., Efstathiou, G., Ellis, R. S., Peterson, B. A., & Shanks, T., 1983, A Complete Galaxy Redshift Sample. I – The Peculiar Velocities between Galaxy Pairs and the Mean Mass Density of the Universe, MNRAS, 205, 605

Blanton, M. R. et al. 2005, New York University Value-Added Galaxy Catalog: A Galaxy Catalog Based on New Public Surveys, AJ, 129, 2562

Bosma, A. 1981, 21-cm Line Studies of Spiral Galaxies. I – Observations of the Galaxies NGC 5033, 3198, 5055, 2841, and 7331, AJ, 86, 1791

Bosma, A. 1981, 21-cm Line Studies of Spiral Galaxies. II – The Distribution and Kinematics of Neutral Hydrogen in Spiral Galaxies of Various Morphological Types, AJ, 86, 1825

Calzetti, D., & Giavalisco, M. 1993, Peculiar velocities and galaxy clustering - Do bulk and shell motions have the same origin?, ApJ, 406, 388

Castro-Rodriguez, N., Ropez-Corredoira, M., Sanchez-Saavedra, M. L., & Battaner, E. 2002, Warps and Correlations with Intrinsic Parameters of Galaxies in the Visible and Radio, A&A, 391, 519

Choi, I. Y., & Ann, H. B. 2011, Spiral Arm Morphology in Cluster Environment, JKAS, 44,161

Choi, Y.-Y., Han, D.-H., & Kim, S. S. 2010, Korea Institute for Advanced Study Value-Added Galaxy Catalog, JKAS, 43,191

Davis, M., Geller, M. J., & Huchra, J. 1978, The Local Mean Mass Density of the Universe – New Methods for Studying Galaxy Clustering, ApJ, 221, 1

Debattista, V. P., & Sellwood, J. A. 1999, Warped Galaxies from Misaligned Angular Momenta, ApJ, 513, L107

Dressler, A. 1980, Galaxy Morphology in Rich Clusters – Implications for the Formation and Evolution of Galaxies, ApJ, 236, 351

Dressler, A., Faber, S. M., Burstein, D., Davies, R. L., Lynden-Bell, D., Terlevich, R. J., & Wegner, G. 1987, Spectroscopy and Photometry of Elliptical Galaxies – A Large-Scale Streaming Motion in the Local Universe, ApJ, 313, 37

Dubinski, J., & Chakrabatry, D. 2009, Warps and Bars from the External Tidal Torques of Tumbling Dark Halos, ApJ, 703, 2068

Fesenko, B. I. 1973, Peculiar Velocities of Galaxies and Indications of the Existence of a Local Cluster, Sov. Astron., 17, 314

Garcia-Ruiz, I., Sancisi, R., & Kuijken, K. 2002. Neutral Hydrogen and Optical Observations of Edge-On Galaxies: Hunting for Warps, A&A 394, 769

Giovanelli, R., Haynes, M. P., Chamaraux, P., Da Costa, L. N., Freudling, W., Salzer, J., & Wegner, G. 1996, Spiral Galaxies and the Peculiar Velocity Field, IAUS, 168, ed. M. Kafatos & Y. Kondo, (Dordrecht: Kluwer), 183

Gomez, F. A., White, S. D. M., Grand, R. J. J., Marinacci, F., Springel, V., & Pakmor, R. 2016, Warps and Waves in Fully Cosmological Models of Galactic Discs, arXiv: 1606.06295

Hawkins, E. et al. 2003, The 2dF Galaxy Redshift Survey: Correlation Functions, Peculiar Velocities and the Matter Density of the Universe, MNRAS, 346, 78

Huang, S., & Carlberg, R. G. 1997, Sinking Satellites and Tilting Disk Galaxies, ApJ, 480, 503

Ideta, M., Hozumi, S., Tsuchiya, T., & Takizawa, M. 2000, Time Evolution of Galactic Warps in Prolate Haloes, MNRAS, 311, 733

Jeon, M., Kim, S. S., & Ann, H. B. 2009, Galactic Warps in Triaxial Halos, ApJ, 696, 1899

Jiang, I., & Binney, J. 1999, Warps and Cosmic Infall, MNRAS, 303, L7

Kalirai, J. S., Guhathakurta, P., Gilbert, K. M., Reitzel, D. B., Majewski, S. R., Rich, R. M., & Cooper, M. C. 2006, Kinematics and Metallicity of M31 Red Giants: The Giant Southern Stream and Discovery of a Second Cold Component at R=20 kpc, ApJ, 641, 268

Karachentsev, I. D. 1971, The Peculiar-Velocity Dispersion of Galaxies, Sov. Astron., 15, 171

Kim, J. H., Peirani, S., Kim, S., Ann, H. B., An, S.-H., & Yoon, S.-J. 2014, Formation of Warped Disks by Galactic Flyby Encounters. I. Stellar Disks, ApJ, 789, 90

Kornreich, D. A., Haynes, M. P., & Lovelace, R. V. E. 1998. Neutral Gas Dynamics of Optically Asymmetric Disk Galaxies, AJ, 116, 21

Kraan-Korteweg, R. C. 1986, A Catalog of 2810 Nearby Galaxies – The Effect of the Virgocentric Flow Model on their Observed Velocities, A&AS, 66, 255

Kuijken, K. 1991, Galactic Disk Warps, ApJ, 376, 467

Lopez-Corredoira, M., Betancort-Rijo, J., & Beckman, J. E. 2002. Generation of Galactic Disc Warps due to Intergalactic Accretion Flows onto the Disc, A&A 386, 169

Lynden-Bell, D. 1965, Free pPrecession for the Galaxy, MNRAS, 129, 299

Lynden-Bell, D., Faber, S. M., Burstein, D., Davies, R. L., Dressler, A., Terlevich, R. J., & Wegner, G. 1988, Spectroscopy and Photometry of Elliptical Galaxies. V – Galaxy Streaming toward the New Supergalactic Center, ApJ, 326, 19

Mould, J. R. et al. 2000, The Hubble Space Telescope Key Project on the Extragalactic Distance Scale. XXVIII. Combining the Constraints on the Hubble Constant, ApJ, 529, 786

Muldrew, S. I. et al. 2012, Measures of Galaxy Environment – I. What is 'Environment'?, MNRAS, 419, 2670

Ostriker, E. C., & Binney, J. 1989, Warped and Tilted Galactic Discs, MNRAS, 237, 785

Peebles, P. J. E. 1979, The Mean Mass Density Estimated from the Kirshner, Oemler, Schechter Galaxy Redshift Sample, AJ, 84, 730

Peebles, P. J. E. 1987, Origin of the Large-Scale Galaxy Peculiar Velocity Field – A Minimal Isocurvature Model, Nature, 327, 210

Quinn, P. J., Hernquist, L., & Fullagar, D. P., 1993, Heating of Galactic Disks by Mergers, ApJ, 403, 74

Raychaudhury, S., & Saslaw, W. C. 1996, The Observed Distribution Function of Peculiar Velocities of Galaxies, ApJ, 461, 514

Reshetnikov, V., Battaner, E. Combes, F., & Jimenez-Vicente, J. 2002, Statistics of Galaxy Warps in the HDF North and South, A&A, 382, 513

Reshetnikov, V., & Combes, F. 1998, Statistics of Optical Warps in Spiral Disks, A&A, 337, 9

Reshetnikov, V., & Combes, F. 1999, Spiral Galaxies with Large Optical Warps, A&A, 138, 101

Reshetnikov, V. P., Mosenkov, A. V., Moiseev, A. V., Kotov, S. S., & Savchenko, S. S. 2016, Galaxies with Conspicuous Optical Warps, MNRAS, 461, 4233

Revaz, Y., & Pfenniger, D. 2004, Bending Instabilities at the Origin of Persistent Warps: A New Constraint on Dark Matter Halos, A&A 425, 67

Rix, H. W., & Zaritsky, D. 1995. Nonaxisymmetric Structures in the Stellar Disks of Galaxies, ApJ, 447, 82

Roskar, R., Debattista, V. P., Brooks, A. M., Quinn, T. R., Brook, C. B., Governato, F., Dalcanton, J. J., & Wadsley, J. 2010, Misaligned Angular Momentum in Hydrodynamic Cosmological Simulations: Warps, Outer Discs and Thick Discs, MNRAS, 408, 783

Saha, K., de Jong R., & Holwerda, B. 2009. The Onset of Warps in Spitzer Observations of Edge-On Spiral Galaxies, MNRAS, 396,409

Sanchez-Saavedra, M. L., Battaner, E., & Florido, E. 1990, Frequency of Warped Spiral Galaxies at Visible Wavelengths, MNRAS, 246, 458

Sanchez-Saavedra, M. L., Battaner, E., Guijarro, A., Lopez-Corredoira, M., & Castro-Rodriguez, N. 2003, A Catalog of Warps in Spiral and Lenticular Galaxies in the Southern Hemisphere, A&A, 399, 457

Sanchez-Martin, P., Romero-Gomez, M., & Masdemont, J. J. 2016, Warp Evidence in Precessing Galactic Bar Models, A&A, 588, 76

Sanchez-Salcedo, F. J. 2006, On the Origin of Warps and the Role of the Intergalactic Medium, MNRAS, 365, 555

Sancisi, R. 1976, Warped HI Disks in Galaxies, A&A, 53, 159

Shen, J., & Sellwood, J. A. 2006, Galactic Warps Induced by Cosmic Infall, MNRAS, 370, 2

Sparke, L. S., & Casertano, S. 1988, A Model for Persistent Galactic Warps, MNRAS, 234, 873

Schwarzkopf, U., & Dettmar, R.-J., 2001. Properties of Tidally-Triggered Vertical Disk Perturbations, A&A, 373, 402.

Tsvetkov, D. Y. 1981, An Estimate for the Typical Peculiar Velocity of Field Galaxies, Sov. Astron., 25, 416

van der Kruit, P. C., & Freeman, K. C. 2011, Galaxy Disks, ARA&A, 49, 301

Wall, J. V., & Jenkins, C. R. 2003, Practical Statistics for Astronomers (Cambridge: Cambridge University Press), 261

Weinberg, M. D., & Blitz, L. 2006, A Magellanic Origin for the Warp of the Galaxy, ApJ, 641, L33

Zaritsky, D., & Rix, H. W. 1997. Lopsided Spiral Galaxies and a Limit on the Galaxy Accretion Rate, ApJ, 477, 118